

Lifshitz phase transitions in the ferromagnetic regime of the Kondo lattice model

Denis Golež¹ and Rok Žitko^{1,2}

¹*Jožef Stefan Institute, Jamova 39, SI-1000 Ljubljana, Slovenia*

²*Faculty for Mathematics and Physics, University of Ljubljana, Jadranska 19, SI-1000 Ljubljana, Slovenia*

(Dated: June 26, 2018)

We establish the low-temperature phase diagrams of the spin-1/2 and spin-1 Kondo lattice models as a function of the conduction-band filling n and the exchange coupling strength J in the regime of ferromagnetic effective exchange interactions ($n \lesssim 0.5$). We show that both models have several distinct ferromagnetic phases separated by continuous Lifshitz transitions of the Fermi-pocket vanishing or emergence type: one of the phases has a true gap in the minority band (half metal), the others only a pseudogap. They can be experimentally distinguished by their magnetization curves; only the gapped phase exhibits magnetization rigidity. We find that, quite generically, ferromagnetism and Kondo screening coexist rather than compete, both in spin-1/2 and spin-1 models. We compute the Curie temperatures and establish a “ferromagnetic Doniach diagram” for both models.

PACS numbers: 71.27.+a, 72.15.Qm, 75.20.Hr, 75.30.Kz, 75.30.Mb

Materials with competing interactions, such as many lanthanide and actinide compounds, have complex low-temperature phase diagrams with different ground states [1–6]. The Kondo lattice model (KLM) [7–9] describes a conduction band of itinerant electrons and a lattice of local moments on f shells, coupled at each site by an antiferromagnetic exchange interaction J . For large J , the moments are screened. The resulting paramagnetic state has Fermi liquid properties with strongly renormalized parameters. For small J , the conduction-band electrons are carriers of long-range magnetic interactions and the moments order. The two regimes are separated by a quantum phase transition at critical J^* , as described by the Doniach diagram [10]. The Néel temperature increases at first quadratically with J , but then it peaks and decreases to zero at J^* as the Kondo screening takes over. The simplest version of the KLM with spin-1/2 moments indeed has an antiferromagnetic (AFM) ground state (Néel order) for small J near half-filling [11, 12]. The nature of the phase transition at J^* has been investigated using a variety of methods, the most accurate of which confirm that the transition is second order (quantum critical) and indicate that it involves a change of the Fermi surface topology [13–15]. In the spin-1 KLM, there is no phase transition at half-filling and the AFM phase extends to large values of J .

While most cerium compounds show AFM order, some are ferromagnetic (FM): CeRu₂Ge₂ [16], CeIn₂ [17, 18], and CeRu₂Al₂B [19]. A number of uranium and neptunium heavy-fermion materials are also FM: UTe [20], UCu_{0.9}Sb₂ [21], UCo_{0.5}Sb₂ [22], NpNiSi₂ [23], Np₂PdGa₃ [24], and UCu₂Si₂ [25]. In addition, there are strong indications of robust coexistence of the Kondo effect and ferromagnetism, in particular in U compounds. In Refs. [25–29] it has been proposed that an appropriate minimal model for this behavior is the spin-1 version of the KLM, where in the mean-field picture the conduction-band electrons underscreen the local moments, while the residual moments order ferromagnetically. FM order appears for low and moderate electron filling n in the conduction band, $n \lesssim 0.5$ [26, 30–33]. Mean-field analy-

sis predicts two phases: for small J the stable phase is a FM regular metal, while for large J there is a transition to a FM heavy metal. Dynamical mean-field theory (DMFT) calculations demonstrated that the spin-1/2 KLM also has a FM order coexisting with (incomplete) Kondo screening [34]. Furthermore, this phase is a half-metal with gapped minority-spin band and a commensurability condition relates the magnetization to filling n [34] due to completely filled minority-spin lower band [2, 35]. A recent mean-field analysis of the spin-1/2 model suggested the presence of several different ferromagnetic phases [37]. So far, however, a single FM phase has been identified in the DMFT calculations [32, 33].

These findings open a number of questions: What is the relationship between ferromagnetism and Kondo screening: do they compete or coexist? What is the minimal model for studying these effects, spin-1/2 or spin-1 KLM? Is there a quantum phase transition between different FM states also in the spin-1/2 model? What is the nature of these transitions and what are their experimental signatures? And, finally, which aspects of the static mean-field analysis [38] are correct and which must be revised in more accurate dynamical treatment? To answer these questions we have performed extensive DMFT [39] calculations using the numerical renormalization group (NRG) as the impurity solver [40–45], as well as static mean-field calculations for both models [38].

We consider the Kondo lattice model

$$\mathcal{H} = \sum_{\mathbf{k}\sigma} (\epsilon_{\mathbf{k}} - \mu) c_{\mathbf{k}\sigma}^\dagger c_{\mathbf{k}\sigma} + J \sum_i \mathbf{s}_i \cdot \mathbf{S}_i, \quad (1)$$

which describes a single-orbital conduction band with dispersion $\omega = \epsilon_{\mathbf{k}}$, and a lattice of local moments described by the spin- S operators \mathbf{S}_i ; \mathbf{s}_i is the conduction-band spin-density at site i , and J is the antiferromagnetic Kondo exchange coupling ($J > 0$). We focus on the Bethe lattice that has a semi-circular density of states with bandwidth $2D$.

In Fig. 1 we present the main result of this work: the phase diagrams of the spin-1/2 and spin-1 KLM as a function of n and J . For *both* spins we find several different ferromagnetic

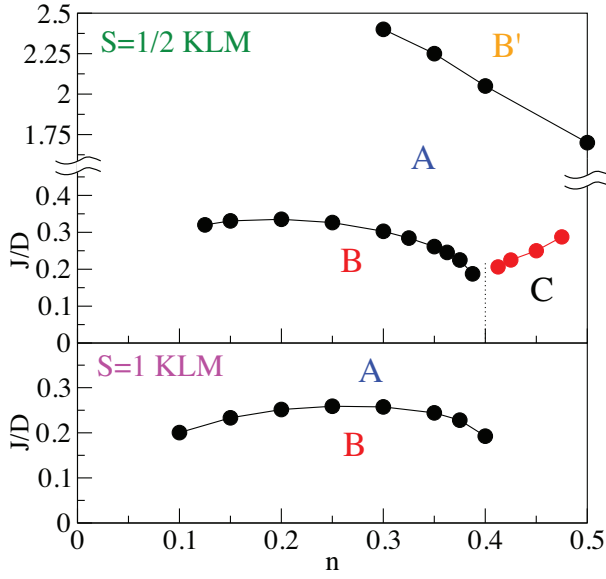


Figure 1: (Color online) Phase diagrams of spin-1/2 and spin-1 Kondo lattice models for $n < 0.5$. Phase A is a ferromagnetic half-metal phase with strong Kondo effect where the minority band is gapped. Phases B and B' are itinerant ferromagnetic phases with a pseudogap. Phase C for spin-1/2 model indicates the region with charge order [46]. For very small n , the calculations fail to converge.

phases. Phase A corresponds to the ferromagnetic half-metal phase described by Peters et al. [34]. The corresponding spin-resolved spectral functions for the $S = 1$ model are shown in Fig. 2, panel A. The minority spin band is gapped [34], while the majority band exhibits the weak hybridization pseudo-gap characteristic of the Kondo lattice systems [47, 48]. Phase B at small J is not gapped, but there is a pronounced pseudogap just below the Fermi level in the minority band, Fig. 2, panel B. The spectral functions for the $S = 1/2$ model are qualitatively the same. The spectra thus suggest the occurrence of a Lifshitz transition at J^* : there is no change in the symmetry, but the Fermi surface of the minority band shrinks to a point and disappears as one goes from phase B to A. We emphasize that the two phases exist both for spin-1/2 and for spin-1 models and have similar properties; clearly, within the DMFT, the value of the spin does not play a crucial role in the BA transition. J^* is a non-monotonic function of n that peaks at $n \sim 0.2$ and $n \sim 0.25$, respectively. Near $n \sim 0.4$ we observe change of behavior in the small- J phase. For $S = 1/2$ KLM, this is the parameter regime where charge order occurs [33, 46], but it is not allowed for in our calculations.

In Fig. 3 we plot the magnetization and the quasiparticle renormalization factor $Z_\sigma = [1 - d\Sigma_\sigma/d\omega(\omega = \mu)]^{-1}$ as a function of J across the BA transition. The frozen magnetization in phase A is given by a generalization of the spin-1/2 KLM result from Refs. [2, 34, 35]:

$$m_S = (2S - n)/2. \quad (2)$$

At transition, the magnetization is continuous with a change of

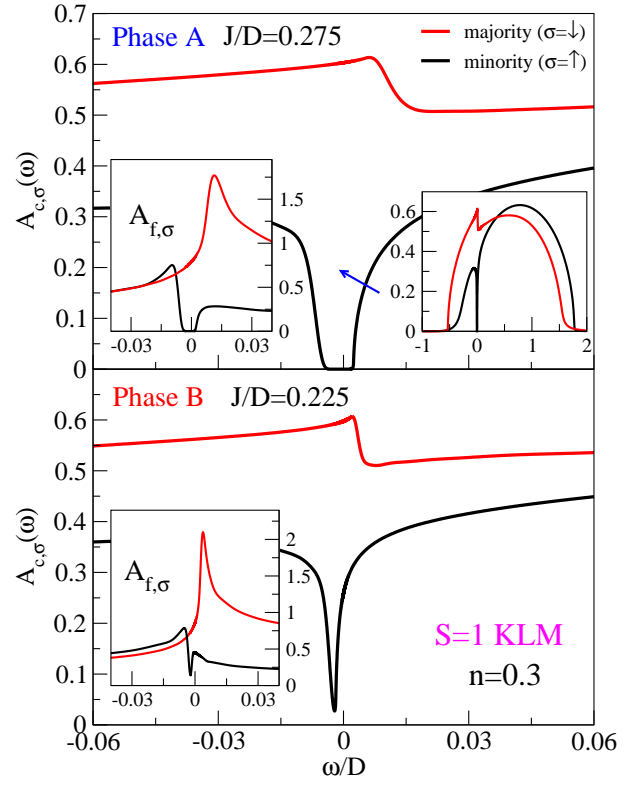


Figure 2: (Color online) Spin-resolved conduction-band local spectral functions $A_{c,\sigma}$ for the spin-1 KLM in the ferromagnetic half-metal phase (A) and in the itinerant ferromagnetic phase (B). The arrow indicates the main effect of decreasing interaction J : the lower edge of the upper hybridized band shifts to lower frequencies. The left insets in both panels show the f -level spectral functions $A_{f,\sigma}$ defined through the imaginary part of the scattering T matrix. The right inset in the upper panel shows the spectral functions in the full frequency interval.

slope in m_f . This is in disagreement with the static mean-field analysis for $S = 1$ which predicts a jump [27]. The factors Z_σ for both spin orientations are continuous and finite across the transition (in the minority band of phase A there are no quasi-particles, but Z_σ can formally still be defined). There is thus no criticality in this spin-selective metal-insulator transition, which may be identified as a *continuous Lifshitz transition of the Fermi pocket vanishing type* [2, 35, 49–52]. The Fermi surface topology is continuous with no reorganization. Deep in the phase A, the majority electrons become weakly correlated (Z has a value of order 0.5).

For very large J , in the spin-1/2 model (but not for spin-1) there is another Lifshitz transition to a non-gapped phase [53] that we denote as B'. While in the BA transition, the chemical potential is located at the *bottom of the upper hybridized band*, in the AB' transition the chemical potential is located at the *top of the lower hybridized band* at the transition point. In other words, while BA corresponds to the vanishing of electron pocket, AB' corresponds to the emergence of hole pocket. For even larger J , the system eventually becomes paramagnetic (for $n = 0.3$ at $J/D = 3.4$).

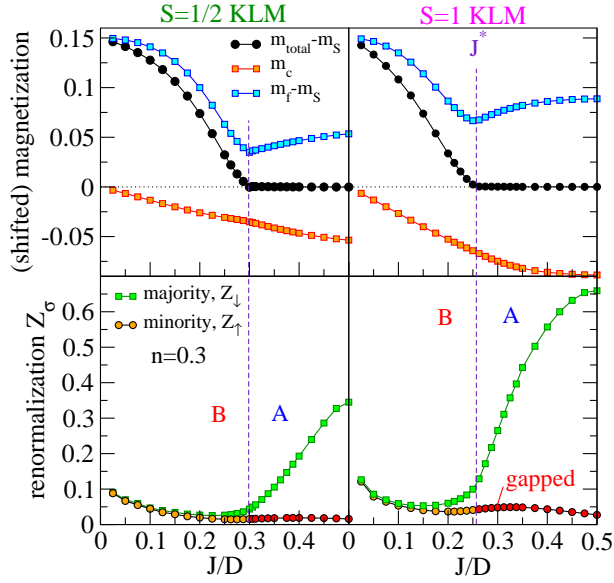


Figure 3: (Color online) Total, conduction-band c -level and localized f -level magnetizations (top panels) and the spin-dependent quasi-particle renormalization factors Z_σ (bottom panels) across the phase transition, indicated by the vertical dashed lines. The magnetization is here defined as the expectation value of the spin operator: $m_f = \langle S_z \rangle$, $m_c = (n_\uparrow - n_\downarrow)/2$, $m_{\text{total}} = m_f + m_c$. In the plots, m_{total} and m_f are shifted by m_S defined in Eq. (2).

The static mean-field theory for $S = 1/2$ also predicts distinct phases [37, 38] which roughly correspond to B, A, and B'. The exact treatment of quantum fluctuations in DMFT leads, however, to a number of differences: i) The small- J phase B is not pure ferromagnetic, but there is a coexistence with the Kondo effect. In the static MF treatment only pure ferromagnetic solution is stable and the phase transition from the corresponding phases A to B is of the first order [51], for details see Supplementary materials [38]. Small- J phase B is not pure ferromagnetic. ii) The Lifshitz transitions are all continuous: there are no jumps in any of the results. iii) Deep inside phases B and B' there are pseudo-gaps rather than gaps. This is due to non-zero imaginary part of the self-energy in DMFT, i.e., due to correlation effects. The most surprising outcome of the DMFT calculations is, in fact, the gradual emergence of true gaps from pseudo-gaps as the gapped phase A is approached from B or from B', while the static MF results are closer to the rigid-band picture.

Does the existence of multiple phases indicate a competition between the exchange interaction and the Kondo effect? Some degree of antagonism is suggested by the fact that the f -shell magnetization m_f has a minimum at the BA Lifshitz point where both tendencies are expected to be equally strong and, furthermore, it could be argued that m_f increases with J in phase A only because Kondo screening is rendered incomplete by the opening and widening of the gap. Nevertheless, this competition does not imply mutual exclusion and most results rather support the notion of robust coexistence.

Experimentally the phases can be distinguished by their

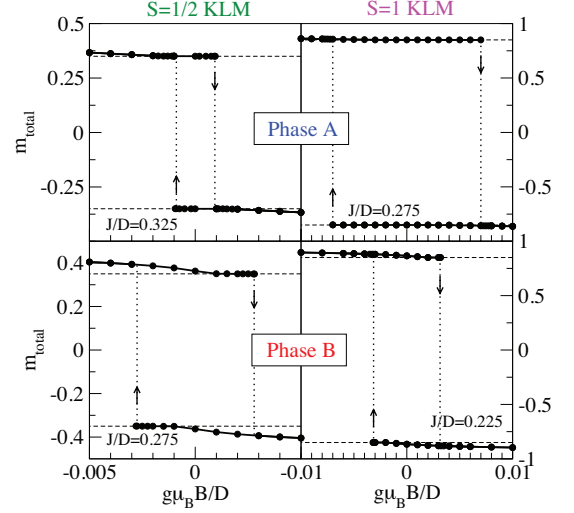


Figure 4: (Color online) Hysteresis loops: magnetization in longitudinal external magnetic field. The dashed lines indicate the value of the frozen magnetization m_S . The g -factors are assumed equal for c and f levels, $g_c = g_f = g$. Occupancy is $n = 0.3$.

magnetization curves. In phase A, m_{total} remains pinned to m_S for a finite range of the field strength, while in phase B the susceptibility dM/dB near zero field is finite, see Fig. 4. For sufficiently strong field, a gap opens in the minority band in phase B, too. This effect can be understood within a rigid-band picture. For very strong field, the magnetization is re-oriented in a first-order spin-flop transition which preempts another Lifshitz transition.

In Fig. 5 we plot the temperature dependence of key thermodynamic and transport properties in phases A and B. We find that the magnetization in phase B remains essentially pinned at m_S until T becomes of the order of the gap, while it has a finite temperature-derivative at $T = 0$ in phase A. This difference is, however, small. The resistance ρ increases in both phases up to the Curie temperature T_c , then it decreases approximately as a power-law $T^{-0.3}$, not logarithmically. The heat capacity c has a jump discontinuity at T_c . Similar features are indeed observed experimentally, for example in Refs. [19, 22, 23], although the simple KLM does not capture the full complexity of real materials.

We summarize the behavior of both Kondo lattice models in the form of a “ferromagnetic Doniach diagram” in Fig. 6. We plot the Kondo temperature for a single-impurity model with flat band (which does not depend on the impurity spin [54]) and the Curie temperature T_C for each model. The Curie temperature has no observable feature at the Lifshitz transition points J^* . Apart from the (approximately) factor of two difference, there is no difference in T_C of spin-1/2 and spin-1 models for small J . At large J , spin-1/2 model first goes into the B' phase and then becomes paramagnetic. The spin-1

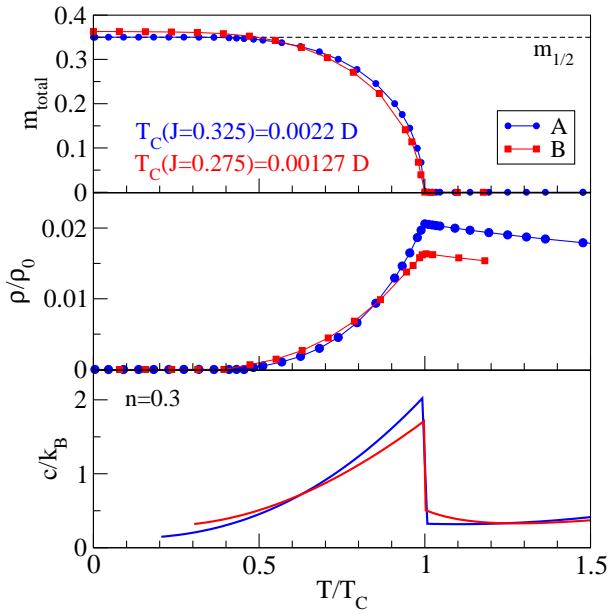


Figure 5: (Color online) Temperature dependence of the magnetization, resistivity and heat capacity for the spin-1/2 Kondo lattice model in phases A and B. The horizontal axis is rescaled by the Curie temperature T_C . Resistivity is in units of $\rho_0 = 2\pi e^2 \Phi(0)/\hbar D$, where Φ is the transport integral. Heat capacity curve was obtained by differentiating a piecewise interpolation of the numerical results for the total energy.

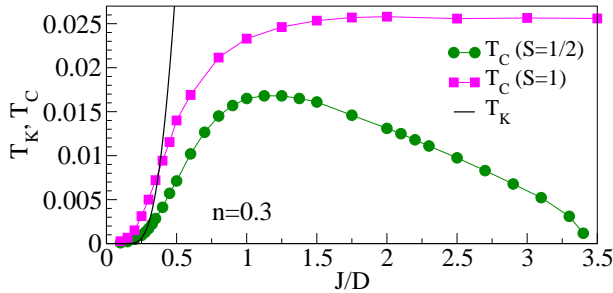


Figure 6: (Color online) “Ferromagnetic Doniach diagram” for spin-1/2 and spin-1 Kondo lattice models.

model remains ferromagnetic in the large J limit. This is similar to the behavior of the AFM phases of both models at half filling.

We conclude by answering the questions raised in the introduction. There is no Kondo breakdown and no criticality, but rather a continuous filling of the lower minority band and the disappearance of the electron pockets (and the emergence of hole pockets in the spin-1/2 model for large J). We find robust coexistence of FM order and Kondo screening in all phases, for both spins. Kondo underscreening does not need to be invoked to explain the magnetic ordering. Both models have qualitatively the same phase diagram for physically most relevant small J . The Lifshitz transitions are observable in the temperature and magnetic-field dependence of the magnetization. The static mean-field appears to be valid at the

qualitative level, however to properly describe the real nature of ferromagnetic phases and transitions it is necessary to take into account dynamic effects, as in the DMFT treatment.

We acknowledge discussions with Robert Peters and Janez Bonča and the support of the Slovenian Research Agency (ARRS) under Program P1-0044.

-
- [1] P. Coleman and A. J. Schofield, *Nature* **433**, 226 (2005).
 - [2] H. Löhneysen, A. Rosch, M. Vojta, and P. Wölfle, *Reviews of Modern Physics* **79**, 1015 (2007).
 - [3] Q. Si and F. Steglich, *Science* **329**, 1161 (2010).
 - [4] G. R. Stewart, *Reviews of Modern Physics* **73**, 797 (2001).
 - [5] P. Gegenwart, Q. Si, and F. Steglich, *Nature Physics* **4**, 186 (2008).
 - [6] C. Pfleiderer, *Reviews of Modern Physics* **81**, 1551 (2009).
 - [7] H. Tsunetsugu, M. Sigrist, and K. Ueda, *Reviews of Modern Physics* **69**, 809 (1997).
 - [8] M. Gulácsi, *Advances in Physics* **53**, 769 (2004).
 - [9] A. C. Hewson, *The Kondo Problem to Heavy-Fermions* (Cambridge University Press, Cambridge, 1993).
 - [10] S. Doniach, *Physica B* **91**, 231 (1977).
 - [11] S. Capponi and F. Assaad, *Physical Review B* **63**, 155114 (2001).
 - [12] J. Otsuki, H. Kusunose, and Y. Kuramoto, *Physical Review Letters* **102**, 017202 (2009).
 - [13] L. De Leo, M. Civelli, and G. Kotliar, *Physical Review Letters* **101**, 256404 (2008).
 - [14] L. Martin and F. Assaad, *Physical Review Letters* **101**, 066404 (2008).
 - [15] L. Martin, M. Bercx, and F. Assaad, *Physical Review B* **82**, 245105 (2010).
 - [16] S. Süllo, M. C. Aronson, B. D. Rainford, and P. Haen, *Physical Review Letters* **82**, 2963 (1999).
 - [17] D. Rojas, J. Espeso, J. Rodríguez Fernández, J. Gómez Sal, J. Sanchez Marcos, and H. Müller, *Physical Review B* **80**, 184413 (2009).
 - [18] K. Mukherjee, K. K. Iyer, and E. V. Sampathkumaran, *Journal of Physics: Condensed Matter* **24**, 096006 (2012).
 - [19] R. Baumbach, H. Chudo, H. Yasuoka, F. Ronning, E. Bauer, and J. Thompson, *Physical Review B* **85**, 094422 (2012).
 - [20] J. Schoenes, B. Frick, and O. Vogt, *Physical Review B* **30**, 6578 (1984).
 - [21] Z. Bukowski, R. Troć, J. Stepień-Damm, C. Sułkowski, and V. H. Tran, *Journal of Alloys and Compounds* **403**, 65 (2005).
 - [22] V. Tran, R. Troć, Z. Bukowski, D. Badurski, and C. Sułkowski, *Physical Review B* **71**, 094428 (2005).
 - [23] E. Colineau, F. Wastin, J. P. Sanchez, and J. Rebizant, *Journal of Physics: Condensed Matter* **20**, 075207 (2008).
 - [24] V. Tran, J. C. Griveau, R. Eloirdi, W. Miiller, and E. Colineau, *Physical Review B* **82**, 094407 (2010).
 - [25] R. Troć, M. Samsel-Czekala, J. Stepień-Damm, and B. Coqblin, *Physical Review B* **85**, 224434 (2012).
 - [26] N. B. Perkins, J. R. Iglesias, M. D. Núñez-Regueiro, and B. Coqblin, *Europhysics Letters (EPL)* **79**, 57006 (2007).
 - [27] N. Perkins, M. Núñez Regueiro, B. Coqblin, and J. Iglesias, *Physical Review B* **76**, 125101 (2007).
 - [28] B. Coqblin, J. R. Iglesias, N. B. Perkins, A. S. d. R. Simoes, and C. Thomas, *Physica B: Condensed Matter* **404**, 2961 (2009).
 - [29] C. Thomas, A. da Rosa Simões, J. Iglesias, C. Lacroix, N. Perkins, and B. Coqblin, *Physical Review B* **83**, 014415 (2011).

- (2011).
- [30] C. Lacroix and M. Cyrot, Physical Review B **20**, 1969 (1979).
 - [31] C. Batista, J. Bonča, and J. Gubernatis, Physical Review Letters **88**, 187203 (2002).
 - [32] R. Peters and T. Pruschke, Phys. Rev. B **76**, 245101 (2007).
 - [33] J. Otsuki, H. Kusunose, and Y. Kuramoto, J. Phys. Soc. Japan **78**, 034719 (2009).
 - [34] R. Peters, N. Kawakami, and T. Pruschke, Phys. Rev. Lett. **108**, 086402 (2012).
 - [35] K. S. D. Beach and F. F. Assaad, Phys. Rev. B **77**, 205123 (2008).
 - [2] S. Viola Kusminskiy, K. Beach, A. Castro Neto, and D. Campbell, Physical Review B **77**, 094419 (2008).
 - [37] Y. Liu, G.-M. Zhang, and L. Yu, *Weak ferromagnetism induced by the Kondo screening effect in the Kondo lattice systems*, condmat:1301.1771 (2013).
 - [38] See supplemental information for a static mean-field analysis of the spin-1/2 and spin-1 Kondo lattice models.
 - [39] A. Georges, G. Kotliar, W. Krauth, and M. J. Rozenberg, Rev. Mod. Phys. **68**, 13 (1996).
 - [40] K. G. Wilson, Rev. Mod. Phys. **47**, 773 (1975).
 - [41] R. Bulla, T. Costi, and T. Pruschke, Rev. Mod. Phys. **80**, 395 (2008).
 - [42] W. Hofstetter, Phys. Rev. Lett. **85**, 1508 (2000).
 - [43] R. Peters, T. Pruschke, and F. B. Anders, Phys. Rev. B **74**, 245114 (2006).
 - [44] A. Weichselbaum and J. von Delft, Phys. Rev. Lett. **99**, 076402 (2007).
 - [45] R. Žitko and T. Pruschke, Phys. Rev. B **79**, 085106 (2009).
 - [46] R. Peters, S. Hashino, N. Kawakami, J. Otsuki, and Y. Kuramoto, *Charge order in kondo lattice systems*, arxiv:1302.5467 (2013).
 - [47] T. Pruschke, R. Bulla, and M. Jarrell, Phys. Rev. B **61**, 12799 (2000).
 - [48] T. A. Costi and N. Manini, J. Low. Temp. Phys. **126**, 835 (2002).
 - [49] I. M. Lifshitz, Sov. Phys. JEPT **11**, 1130 (1960).
 - [50] Y. Yamaji, T. Misawa, and M. Imada, Journal of the Physical Society of Japan **75**, 094719 (2006).
 - [51] G.-B. Li, G.-M. Zhang, and L. Yu, Physical Review B **81**, 094420 (2010).
 - [52] M. Bercx and F. F. Assaad, Phys. Rev. B **86**, 075108 (2012).
 - [53] R. Peters, Private communication.
 - [54] N. Andrei, K. Furuya, and J. H. Lowenstein, Rev. Mod. Phys. **55**, 331 (1983).

Supplemental Material

Static mean-field theory

The $S = 1/2$ case

We perform a mean-field decomposition in the KLM written in the form:

$$\mathcal{H} = \sum_{k,\sigma} \epsilon_k c_{k,\sigma}^\dagger c_{k,\sigma} + J \sum_i \mathbf{s}_i \cdot \mathbf{S}_i + \mu_B H \sum_i (g_c s_{z,i} + g_f S_{z,i}), \quad (\text{A.3})$$

where H is the external magnetic field oriented along the z axis, μ_B the Bohr magneton, while g_c and g_f are the Landé factors. For simplicity, we consider flat non-interacting conduction-band density of states (DOS):

$$\rho_c^0 = 1/2D, \quad (\text{A.4})$$

where D is the half-bandwidth.

The interaction term for localized spins with $S = 1/2$ is decomposed in terms of the hybridization operators [1, 2]

$$\chi^\mu = \frac{1}{\sqrt{2}} \sum_{\alpha,\beta} f_\alpha^\dagger \sigma_{\alpha\beta}^\mu c_\beta, \quad (\text{A.5})$$

where c, f are annihilation operators for itinerant and localized electrons, respectively, and the spin indexes α and β range over spin up and down. The index μ ranges over 0, 1, 2, 3; the operator σ^0 is the identity, while other σ^i are the Pauli matrices. These operators are complete in the spin sector $1/2 \otimes 1/2 = 1 \oplus 0$, and therefore the interaction part can be split into:

$$\mathbf{s} \cdot \mathbf{S} = \left(\frac{1}{2} c^\dagger \boldsymbol{\sigma} c \right) \cdot \left(\frac{1}{2} f^\dagger \boldsymbol{\sigma} f \right) = -3/4 \chi^{0\dagger} \chi^0 + 1/4 \boldsymbol{\chi}^\dagger \cdot \boldsymbol{\chi}. \quad (\text{A.6})$$

This expression is exact.

We perform the standard mean-field procedure: $AB \approx \langle A \rangle B + A \langle B \rangle - \langle A \rangle \langle B \rangle$. We assume that only the singlet part $\langle \chi^0 \rangle$ is nonzero and we use the $U(1)$ gauge freedom to make $\langle \chi_0 \rangle$ real.

The second mean-field decomposition is done in the magnetic channel (assuming the magnetization is along the z axis):

$$\mathbf{s} \cdot \mathbf{S} = s_z \tilde{m}_f + \tilde{m}_c S_z - \tilde{m}_c \tilde{m}_f, \quad (\text{A.7})$$

where

$$\tilde{m}_c = \langle s^z \rangle \quad \text{and} \quad \tilde{m}_f = \langle S^z \rangle \quad (\text{A.8})$$

are the expectation values of the z component of conduction-band and localized-electron spin. These are proportional to the magnetization of $c(f)$ electrons:

$$m_{f(c)} = -\mu_B g_{f(c)} \tilde{m}_{f(c)}. \quad (\text{A.9})$$

In order to fix the average number of electrons we introduce the chemical potential μ . We also introduce Lagrangian multipliers λ_i to enforce the local constraint $\langle n_{f,i} \rangle = 1$ on the f electrons:

$$\sum_i \lambda_i \sum_\sigma \left(f_{i,\sigma}^\dagger f_{i,\sigma} - 1 \right). \quad (\text{A.10})$$

This constraint is fulfilled only as an average over all f electrons, $\lambda_i \equiv \lambda$. We may then perform a FT:

$$\lambda \sum_k \sum_\sigma \left(f_{k\sigma}^\dagger f_{k\sigma} - 1 \right). \quad (\text{A.11})$$

Thus λ plays the role of the effective f level energy: the f level occupancy is controlled by the difference between λ and μ .

At constant μ , the thermodynamic potential that we need to minimize is

$$K(\mu, \dots) = H(N_{\text{total}}, \dots) - \mu N_{\text{total}} = H - \mu(N_c + N_f) = H - \mu \sum_{k,\sigma} \left(c_{k\sigma}^\dagger c_{k\sigma} + f_{k\sigma}^\dagger f_{k\sigma} \right). \quad (\text{A.12})$$

The mean-field thermodynamic potential takes the following wave-vector representation:

$$\mathcal{K}_{MF} = \sum_{k\sigma} \begin{pmatrix} c_{k,\sigma}^\dagger & f_{k,\sigma}^\dagger \end{pmatrix} \tilde{M}_k \begin{pmatrix} c_{k,\sigma} \\ f_{k,\sigma} \end{pmatrix} + \sum_k E_0, \quad (\text{A.13})$$

where the matrix M_k is

$$\tilde{M}_k = \begin{pmatrix} \epsilon_{k,\sigma} - \mu & -c\chi_0 \\ -c\chi_0 & \lambda_\sigma - \mu \end{pmatrix}. \quad (\text{A.14})$$

with

$$\epsilon_{k,\sigma} = \epsilon_k + \epsilon_\sigma = \epsilon_k + J\tilde{m}_f \frac{\sigma}{2} + \mu_B g_c H \frac{\sigma}{2} = \epsilon_k + \mu_B g_c \tilde{H}_c \frac{\sigma}{2}, \quad (\text{A.15})$$

$$\lambda_\sigma = \lambda + J\tilde{m}_c \frac{\sigma}{2} + \mu_B g_f H \frac{\sigma}{2} = \lambda + \mu_B g_f \tilde{H}_f \frac{\sigma}{2}, \quad (\text{A.16})$$

$$c = \frac{3}{4} \frac{1}{\sqrt{2}} J = \frac{3J}{4\sqrt{2}}, \quad (\text{A.17})$$

$$E_0 = +\frac{3}{4} J \chi_0^2 - J \tilde{m}_c \tilde{m}_f - \lambda. \quad (\text{A.18})$$

The effective field felt by the $c(f)$ electrons is given by

$$\tilde{H}_{c(f)} = H + \frac{J\tilde{m}_{f(c)}}{\mu_B g_{c(f)}}. \quad (\text{A.19})$$

In general, the equation of motion (EOM) can be written as

$$z \langle \langle A, B \rangle \rangle = -\langle \langle [\mathcal{K}_{MF}, A], B \rangle \rangle + \langle \langle [A, B] \rangle \rangle, \quad (\text{A.20})$$

where A, B are arbitrary fermionic operators. We find

$$\begin{aligned} zG_{cc,k\sigma} &= 1 + (\epsilon_{k\sigma} - \mu) G_{cc,k\sigma} - c\chi_0 G_{fc,k\sigma}, \\ zG_{ff,k\sigma} &= 1 + (\lambda_\sigma - \mu) G_{ff,k\sigma} - c\chi_0 G_{cf,k\sigma}, \\ zG_{cf,k\sigma} &= (\epsilon_{k\sigma} - \mu) G_{cf,k\sigma} - c\chi_0 G_{ff,k\sigma}, \\ zG_{fc,k\sigma} &= (\lambda_\sigma - \mu) G_{fc,k\sigma} - c\chi_0 G_{cc,k\sigma}. \end{aligned} \quad (\text{A.21})$$

Note also that $G_{cf}(z) = G_{fc}(z)$, since the matrix \tilde{M}_k is symmetric. It follows

$$\begin{aligned} (z - \epsilon_{k\sigma} + \mu) G_{cc,k\sigma} &= 1 - c\chi_0 G_{fc,k\sigma}, \\ (z - \lambda_\sigma + \mu) G_{ff,k\sigma} &= 1 - c\chi_0 G_{cf,k\sigma}, \\ (z - \epsilon_{k\sigma} + \mu) G_{cf,k\sigma} &= -c\chi_0 G_{ff,k\sigma}, \\ (z - \lambda_\sigma + \mu) G_{fc,k\sigma} &= -c\chi_0 G_{cc,k\sigma}, \end{aligned} \quad (\text{A.22})$$

and consequently

$$(z - \lambda_\sigma + \mu)^2 G_{ff,k\sigma} = (c\chi_0)^2 G_{cc,k\sigma}. \quad (\text{A.23})$$

In this approach, writing $z = \omega + i\delta$, the Fermi level corresponds to $\omega = 0$. We use a different convention. We absorb μ into z : $\tilde{z} = z + \mu$. Also the Green's functions take \tilde{z} as their argument. With this choice, spectral functions are obtained with replacement $\tilde{z} = \omega + i\delta$ and there are no explicit μ in the expressions for Green's functions. μ only appears as an integration limit (or in the Fermi-Dirac distribution). We drop writing the tilde in \tilde{z} in the following.

The quasiparticle band edges are

$$\begin{aligned}\omega_{1,\sigma} &= \frac{1}{2} \left(\epsilon_\sigma + \lambda_\sigma - D - \sqrt{(\epsilon_\sigma - \lambda_\sigma - D)^2 + 4c^2\chi_0^2} \right), \\ \omega_{2,\sigma} &= \frac{1}{2} \left(\epsilon_\sigma + \lambda_\sigma + D - \sqrt{(\epsilon_\sigma - \lambda_\sigma + D)^2 + 4c^2\chi_0^2} \right), \\ \omega_{3,\sigma} &= \frac{1}{2} \left(\epsilon_\sigma + \lambda_\sigma - D + \sqrt{(\epsilon_\sigma - \lambda_\sigma - D)^2 + 4c^2\chi_0^2} \right), \\ \omega_{4,\sigma} &= \frac{1}{2} \left(\epsilon_\sigma + \lambda_\sigma + D + \sqrt{(\epsilon_\sigma - \lambda_\sigma + D)^2 + 4c^2\chi_0^2} \right).\end{aligned}\tag{A.24}$$

In the multiindex (i, σ) , σ is spin, while i enumerates the band edges from the lowest to the highest. Furthermore

$$\epsilon_\sigma = J\tilde{m}_f \frac{\sigma}{2} + \mu_B g_c H \frac{\sigma}{2} = \mu_B g_c \tilde{H}_c \frac{\sigma}{2}.\tag{A.25}$$

The final closed-form expressions for the spectral functions are

$$\rho_{c,\sigma}(\omega) = \rho_c^0 \sum_{i=1}^4 (-1)^{i-1} \theta(\omega - \omega_{i,\sigma}),\tag{A.26}$$

$$\rho_{f,\sigma}(\omega) = \frac{(c\chi_0)^2}{(\omega - \lambda_\sigma)^2} \rho_{c,\sigma}(\omega).\tag{A.27}$$

We also have

$$\rho_{cf,\sigma}(\omega) = -\frac{c\chi_0}{\omega - \lambda_\sigma} \rho_{c,\sigma}(\omega).\tag{A.28}$$

The energy eigenvalues are

$$E_{k,\sigma} = \frac{1}{2} \left(\epsilon_{k,\sigma} + \lambda_\sigma \pm \sqrt{(\epsilon_{k,\sigma} - \lambda_\sigma)^2 + 4c^2\chi_0^2} \right).\tag{A.29}$$

Mean-field equations

We can derive the system of mean-field equation using the fluctuation-dissipation theorem at $T = 0$:

$$\begin{aligned}\langle AB \rangle &= - \int_{\mu}^{\infty} \frac{d\omega}{\pi} G''_{AB}(\omega) \\ &= \int_{-\infty}^{\mu} d\omega \rho_{BA}(\omega).\end{aligned}\tag{A.30}$$

We obtain

$$n_c = \sum_{\sigma} \langle c_{\sigma}^{\dagger} c_{\sigma} \rangle = \sum_{\sigma} \int d\omega \rho_{c,\sigma}(\omega),\tag{A.31}$$

$$1 = n_f = \sum_{\sigma} \langle f_{\sigma}^{\dagger} f_{\sigma} \rangle = \sum_{\sigma} \int d\omega \rho_{f,\sigma}(\omega),\tag{A.32}$$

$$\tilde{m}_c = 1/2 \sum_{\sigma} \sigma \langle c_{\sigma}^{\dagger} c_{\sigma} \rangle = 1/2 \sum_{\sigma} \int \sigma d\omega \rho_{c,\sigma}(\omega),\tag{A.33}$$

$$\tilde{m}_f = 1/2 \sum_{\sigma} \sigma \langle f_{\sigma}^{\dagger} f_{\sigma} \rangle = 1/2 \sum_{\sigma} \int \sigma d\omega \rho_{f,\sigma}(\omega).\tag{A.34}$$

In all integrals, the lower integration limit is $-\infty$, while the upper is the chemical potential μ .

For the gap equation we take the symmetrized spectral function

$$A_{cf,\sigma} = -\frac{1}{2\pi}[\text{Im}G_{cf}(\omega + i\delta) + \text{Im}G_{fc}(\omega + i\delta)] = \rho_{cf,\sigma}.$$

This gives:

$$\frac{1}{2}\langle f_{\uparrow}^{\dagger}c_{\uparrow} + c_{\uparrow}^{\dagger}f_{\uparrow} + f_{\downarrow}^{\dagger}c_{\downarrow} + c_{\downarrow}^{\dagger}f_{\downarrow} \rangle = \frac{1}{2}2\sqrt{2}\langle\chi_0\rangle = \quad (\text{A.35})$$

$$\sum_{\sigma} \int d\omega A_{fc,\sigma}(\omega) = -c\chi_0 \sum_{\sigma} \int d\omega \frac{1}{\omega - \lambda_{\sigma}} \rho_{c,\sigma}(\omega) \quad (\text{A.36})$$

We now assume $\chi_0 \neq 0$. Using $c = 3J/(4\sqrt{2})$, we finally find the gap equation

$$\boxed{\sum_{\sigma} \int_{-\infty}^{\mu} d\omega \frac{\rho_{c,\sigma}(\omega)}{\omega - \lambda_{\sigma}} = -8/3J.} \quad (\text{A.37})$$

This set of non-linear equations had been previously derived in Refs. [1, 2], while in Ref. [3] a somewhat different mean-field decoupling was used.

Evaluation of energy

The total energy can be evaluated as

$$\begin{aligned} E_{\text{GS}} &= \langle H_{\text{MF}} \rangle \\ &= \sum_k \left\langle \sum_{ij} c_{ki}^{\dagger} c_{kj} M_{k,ij} + E_0 \right\rangle \\ &= \sum_k \left(\sum_{ij} \int_{-\infty}^{\mu} A_{\epsilon_k,ij}(\omega) M_{\epsilon_k,ij} d\omega + E_0 \right). \end{aligned} \quad (\text{A.38})$$

We used a symmetrized spectral function

$$A_{ij}(\omega) = \frac{1}{2} \left[-\frac{1}{\pi} \text{Im}G_{ij}(\omega + i\delta) - \frac{1}{\pi} \text{Im}G_{ji}(\omega + i\delta) \right], \quad (\text{A.39})$$

since

$$\int_{-\infty}^{\mu} A_{ij}(\omega) d\omega = \frac{1}{2} \langle c_i^{\dagger} c_j + c_j^{\dagger} c_i \rangle. \quad (\text{A.40})$$

Then

$$\frac{E_{\text{GS}}}{N} = E_0 + \int_{-D}^D \rho(\epsilon) d\epsilon \int_{-\infty}^{\mu} \text{Tr}[\mathbf{A}_{\epsilon}(\omega) \mathbf{M}_{\epsilon}] d\omega. \quad (\text{A.41})$$

Note that both \mathbf{A} and \mathbf{M} have out-of-diagonal matrix elements. Now we use

$$\text{Tr}[\mathbf{A}(\omega) \mathbf{M}] = -\frac{1}{\pi} \text{Im} \text{Tr}[\mathbf{G}(\omega + i\delta) \mathbf{M}] = -\frac{1}{\pi} \text{Im} \text{Tr}[(\omega + i\delta - \mathbf{M})^{-1} \mathbf{M}] = -\frac{1}{\pi} \text{Im} \text{Tr}[(\omega + i\delta - \mathbf{M})^{-1} \omega] = \text{Tr}[\mathbf{A}(\omega)] \omega, \quad (\text{A.42})$$

which follows from the fact that $\text{Im}[1/(z - x)]$ is a delta distribution, and we have used a transformation to the eigenbasis and back to replace \mathbf{M} by ω in the third step. Thus, after the integration over ϵ ,

$$\frac{E_{\text{GS}}}{N} = E_0 + \sum_{\sigma} \int_{-\infty}^{\mu} \omega d\omega [\rho_{c,\sigma}(\omega) + \rho_{f,\sigma}(\omega)]. \quad (\text{A.43})$$

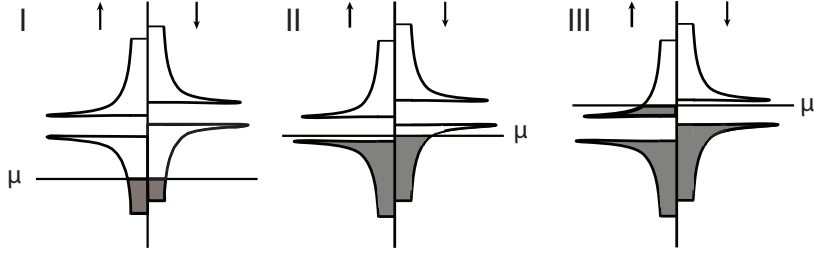


Figure 7: Sketch of the possible placements of the bands with respect to the chemical potential. The phase I correspond to the phase B', phase II to the phase A and phase III to the phase B in the DMFT calculations.

We also have

$$\begin{aligned} \frac{N_c + N_f}{N} &= \int_{-D}^D \rho(\epsilon) d\epsilon \int_{-\infty}^{\mu} \text{Tr}[A_{\epsilon}(\omega)] d\omega \\ &= \sum_{\sigma} \int_{-\infty}^{\mu} [\rho_{c,\sigma}(\omega) + \rho_{f,\sigma}(\omega)] d\omega, \end{aligned} \quad (\text{A.44})$$

thus finally,

$$\frac{K_{GS}}{N} = E_0 + \sum_{\sigma} \int_{-\infty}^{\mu} d\omega (\omega - \mu) [\rho_{c,\sigma}(\omega) + \rho_{f,\sigma}(\omega)]. \quad (\text{A.45})$$

We would like to evaluate Eq. (A.45) for two different cases represented on Fig. 7, namely cases I and II:

$$\begin{aligned} \frac{K_{GS}}{N} &= E_0 + \sum_{\sigma} \int_{-\infty}^{\mu} d\omega (\omega - \mu) \left(1 + \frac{(c\chi_0)^2}{(\omega - \lambda_{\sigma})^2} \right) \rho_{c\sigma}(\omega) \\ &= E_0 + E_c + (c\chi_0)^2 \sum_{\sigma} \int_{-\infty}^{\mu} d\omega \frac{\omega - \lambda_{\sigma} + \lambda_{\sigma} - \mu}{(\omega - \lambda_{\sigma})^2} \rho_{c\sigma}(\omega) \\ &= E_0 + E_c + (c\chi_0)^2 \sum_{\sigma} \int_{-\infty}^{\mu} d\omega \frac{\rho_{c,\sigma}(\omega)}{\omega - \lambda_{\sigma}} + \sum_{\sigma} (\lambda_{\sigma} - \mu) n_{f,\sigma} \\ &= E_0 + E_c + (c\chi_0)^2 (-8/3J) + \sum_{\sigma} (\lambda_{\sigma} - \mu) n_{f,\sigma}, \end{aligned} \quad (\text{A.46})$$

where $E_c = \int_{-\infty}^{\mu} d\omega (\omega - \mu) \rho_{c,\sigma}(\omega)$ and in the last line we have use the gap equation, see Eq. (A.37). We need to evaluate

$$\begin{aligned} 2 \sum_{\sigma} (\lambda_{\sigma} - \mu) n_{f,\sigma} &= \sum_{\sigma} \left(\lambda - \mu + \mu_B g_f \tilde{H}_f \frac{\sigma}{2} \right) n_{f\sigma} \\ &= (\lambda - \mu) n_f + 2\mu_B g_f \tilde{H}_f \tilde{m}_f. \end{aligned} \quad (\text{A.47})$$

For $H = 0$, this is equal to

$$(\lambda - \mu) n_f + J \tilde{m}_c \tilde{m}_f. \quad (\text{A.48})$$

Case I is when $\omega_{1,\sigma} < \mu < \omega_{2,\sigma}$ for both spin orientations. We can write:

$$E_c = \rho_{c,0} \sum_{\sigma} [(\mu^2 - \omega_{1,\sigma}^2)/2] - \mu n_c \quad (\text{A.49})$$

and

$$\begin{aligned} \frac{K_{GS}}{N} &= \frac{3}{4} J \chi_0^2 - J \tilde{m}_c \tilde{m}_f - \lambda + \rho_{c,0} \sum_{\sigma} [(\mu^2 - \omega_{1,\sigma}^2)/2] - \mu n_c - \frac{3}{4} J \chi_0^2 + \sum_{\sigma} (\lambda_{\sigma} - \mu) n_{f,\sigma} \\ &= -J \tilde{m}_c \tilde{m}_f - \lambda + \rho_{c,0} \sum_{\sigma} [(\mu^2 - \omega_{1,\sigma}^2)/2] - \mu n_c + (\lambda - \mu) n_f + J \tilde{m}_c \tilde{m}_f \\ &= \rho_{c,0} \sum_{\sigma} [(\mu^2 - \omega_{1,\sigma}^2)/2] - \mu [n_c + n_f] \end{aligned} \quad (\text{A.50})$$

where in the second line we have used Eq. (A.48) and in the last line $\langle n_f \rangle = 1$.

Case II is when $\omega_{2,\uparrow} < \mu < \omega_{3,\uparrow}$ and only difference is that $\mu \rightarrow \omega_{2,\uparrow}$ in integration limit for \uparrow c electrons. Therefore, the only difference is in the evaluation of E_c :

$$E_c = \rho_c^0 \left(\frac{\mu^2 - \omega_{1,\downarrow}^2}{2} + \frac{\omega_{2,\uparrow}^2 - \omega_{1,\uparrow}^2}{2} \right) - \mu n_c. \quad (\text{A.51})$$

The $S = 1$ case

We next proceed with an analogous treatment for the $S = 1$ problem. We decompose the interaction term into doublet and quadruplet terms, $1/2 \otimes 1 = 1/2 \oplus 3/2$. We find:

$$\mathbf{s} \cdot \mathbf{S} = - \sum_{i=1}^2 \chi_{d,i}^\dagger \chi_{d,i} + (1/2) \sum_{i=1}^4 \chi_{q,i}^\dagger \chi_{q,i}, \quad (\text{A.52})$$

where $\chi_{d,i}(\chi_{q,j})$ are the doublet ($i = 1, 2$) and the quadruplet ($j = 1, 2, 3, 4$) sets of operators under the spin $SU(2)$ symmetry, namely:

$$\chi_{d,1} = -\sqrt{1/3}c_{\downarrow}^\dagger f_0 - \sqrt{2/3}c_{\uparrow}^\dagger f_1, \quad \chi_{d,2} = \sqrt{2/3}c_{\downarrow}^\dagger f_{-1} + \sqrt{1/3}c_{\uparrow}^\dagger f_0, \quad (\text{A.53})$$

$$\chi_{q,1} = -c_{\uparrow}^\dagger f_{-1}, \quad \chi_{q,2} = -\sqrt{1/3}c_{\downarrow}^\dagger f_{-1} + \sqrt{2/3}c_{\uparrow}^\dagger f_0, \quad \chi_{q,3} = \sqrt{2/3}c_{\downarrow}^\dagger f_0 - \sqrt{1/3}c_{\uparrow}^\dagger f_1, \quad \chi_{q,4} = -c_{\downarrow}^\dagger f_1. \quad (\text{A.54})$$

These operators again form a complete set in the spin sector. The decomposition in Eq. (A.52) is exact.

We focus on the doublet part and set all quadruplet fields to zero, $\langle \chi_{q,j} \rangle = 0$. We explicitly break the $SU(2)$ symmetry by setting $\langle \chi_{d,2} \rangle = 0$ and use the $U(1)$ gauge freedom to make $\langle \chi_{d,1} \rangle$ real. In analogy with the $S = 1/2$ case, we make a second mean-field decomposition in the magnetic channel. The mean-field Hamiltonian has a simple wave-vector representation:

$$\mathcal{K}_{MF} = \sum_k \left(c_{k,\downarrow}^\dagger c_{k,\uparrow}^\dagger f_{k,-1}^\dagger f_{k,0}^\dagger f_{k,+1}^\dagger \right) \tilde{M}_k \begin{pmatrix} c_{k,\downarrow} \\ c_{k,\uparrow} \\ f_{k,-1} \\ f_{k,0} \\ f_{k,+1} \end{pmatrix} + \sum_k E_0, \quad (\text{A.55})$$

where the matrix \tilde{M}_k is

$$\begin{pmatrix} \epsilon_{k,\downarrow} - \mu & 0 & 0 & J\chi_{d,1}/\sqrt{3} & 0 \\ 0 & \epsilon_{k,\uparrow} - \mu & 0 & 0 & \sqrt{2/3}J\chi_{d,1} \\ 0 & 0 & \lambda_{-1} - \mu & 0 & 0 \\ J\chi_{d,1}/\sqrt{3} & 0 & 0 & \lambda_0 - \mu & 0 \\ 0 & \sqrt{2/3}J\chi_{d,1} & 0 & 0 & \lambda_1 - \mu \end{pmatrix} \quad (\text{A.56})$$

and

$$\epsilon_{k,\sigma} = \epsilon_k + J\tilde{m}_f \frac{\sigma}{2} + \mu_B g_c H \frac{\sigma}{2} = \epsilon_k + \mu_B g_c \tilde{H}_c \frac{\sigma}{2}, \quad (\text{A.57})$$

$$\lambda_i = \lambda + J\tilde{m}_c i + \mu_B g_f H i = \lambda + \mu_B g_f \tilde{H}_f i, \quad (\text{A.58})$$

$$E_0 = J\chi_{d,1}^2 - J\tilde{m}_c \tilde{m}_f - \lambda, \quad (\text{A.59})$$

with $\sigma = \pm 1$, $i = -1, 0, 1$. The effective field felt by the $c(f)$ electrons is given by

$$\tilde{H}_{c(f)} = H + \frac{J\tilde{m}_{f(c)}}{\mu_B g_{c(f)}}. \quad (\text{A.60})$$

The EOMs are

$$\begin{aligned}
(z - \epsilon_{k,\downarrow} + \mu)G_{c\downarrow,k} &= 1 + \sqrt{\frac{1}{3}}J\chi_{d1}G_{f_0,c\downarrow,k} \\
(z - \epsilon_{k,\uparrow} + \mu)G_{c\uparrow,k} &= 1 + \sqrt{\frac{2}{3}}J\chi_{d1}G_{f_1,c\uparrow,k} \\
(z - \lambda_{-1} + \mu)G_{f_{-1},k} &= 1 \\
(z - \lambda_0 + \mu)G_{f_0,c\downarrow,k} &= \sqrt{\frac{1}{3}}J\chi_{d1}G_{c\downarrow,c\downarrow,k} \\
(z - \epsilon_{k,\downarrow} + \mu)G_{c\downarrow f_0,k} &= \sqrt{\frac{1}{3}}J\chi_{d1}G_{f_0,f_0,k}
\end{aligned} \tag{A.61}$$

and note also that $G_{ij,k}(z) = G_{ji,k}(z)$, while for the diagonal elements we used $G_{ii,k}(z) = G_{i,k}(z)$. Consequently

$$\begin{aligned}
(z - \lambda_0 + \mu)^2 G_{f_0,k} &= (z - \lambda_0 + \mu) \left(1 + \frac{(J\chi_{d1})^2}{3} G_{c\downarrow,k} \right) \\
(z - \lambda_1 + \mu)^2 G_{f_1,k} &= (z - \lambda_1 + \mu) \left(1 + \frac{2(J\chi_{d1})^2}{3} G_{c\uparrow,k} \right).
\end{aligned} \tag{A.62}$$

Once more we absorb μ into z : $\tilde{z} = z + \mu$ and drop writing tilde in \tilde{z} in the following. The quasiparticles band edges $\omega_{i,\sigma}$ are:

$$\begin{aligned}
\omega_{1,\sigma} &= \left(3\epsilon_\sigma - 3D + 3\lambda_\sigma - \sqrt{9(\epsilon_\sigma - D - \lambda_\sigma)^2 + 12F_\sigma(J\chi_{d,1})^2} \right) / 6 \\
\omega_{2,\sigma} &= \left(3\epsilon_\sigma + 3D + 3\lambda_\sigma - \sqrt{9(\epsilon_\sigma + D - \lambda_\sigma)^2 + 12F_\sigma(J\chi_{d,1})^2} \right) / 6 \\
\omega_{3,\sigma} &= \left(3\epsilon_\sigma - 3D + 3\lambda_\sigma + \sqrt{9(\epsilon_\sigma - D - \lambda_\sigma)^2 + 12F_\sigma(J\chi_{d,1})^2} \right) / 6 \\
\omega_{4,\sigma} &= \left(3\epsilon_\sigma + 3D + 3\lambda_\sigma + \sqrt{9(\epsilon_\sigma + D - \lambda_\sigma)^2 + 12F_\sigma(J\chi_{d,1})^2} \right) / 6,
\end{aligned} \tag{A.63}$$

where ϵ_σ has been defined in the section on the $S = 1/2$ model, while

$$F(1) = 2, \quad F(-1) = 1. \tag{A.64}$$

and, furthermore,

$$\lambda_\downarrow = \lambda_0, \tag{A.65}$$

$$\lambda_\uparrow = \lambda_1. \tag{A.66}$$

The spectral functions are given by:

$$\rho_{c,\sigma}(\omega) = \rho_c^0 \sum_{i=1}^4 (-1)^{i-1} \theta(\omega - \omega_{i,\sigma}), \tag{A.67}$$

$$\rho_{f,-1}(\omega) = \delta(\omega - \lambda_{-1}), \tag{A.68}$$

$$\rho_{f,0}(\omega) = F_{-1} \frac{(J\chi_{d,1})^2}{3(z - \lambda_0)^2} \rho_{c,\downarrow}(\omega), \tag{A.69}$$

$$\rho_{f,1}(\omega) = F_1 \frac{(J\chi_{d,1})^2}{3(z - \lambda_1)^2} \rho_{c,\uparrow}(\omega). \tag{A.70}$$

$$\rho_{f_1 c_\uparrow}(\omega) = \sqrt{\frac{2}{3}} \frac{(J\chi_{d,1})}{(\omega - \lambda_1)} \rho_{c_\uparrow}(\omega). \quad (\text{A.71})$$

$$\rho_{f_0 c_\downarrow}(\omega) = \sqrt{\frac{1}{3}} \frac{(J\chi_{d,1})}{(\omega - \lambda_0)} \rho_{c_\downarrow}(\omega). \quad (\text{A.72})$$

The f_{-1} must be unoccupied, otherwise the number of f electrons cannot be exactly 1. Thus $\lambda_{-1} > \mu$. This also implies that f_{-1} must be the highest in energy of the f states, thus $\tilde{m}_c < 0$ and consequently $\tilde{m}_f > 0$.

The mean-field equations

Using the fluctuation-dissipation theorem at $T = 0$, we find

$$n_c = \sum_{\sigma} \langle c_{\sigma}^{\dagger} c_{\sigma} \rangle = \sum_{\sigma} \int d\omega \rho_{c,\sigma}(\omega), \quad (\text{A.73})$$

$$1 = n_f = \sum_i \langle f_i^{\dagger} f_i \rangle = \sum_i \int d\omega \rho_{f,i}(\omega), \quad (\text{A.74})$$

$$\tilde{m}_c = 1/2 \sum_{\sigma} \sigma \langle c_{\sigma}^{\dagger} c_{\sigma} \rangle = 1/2 \sum_{\sigma} \int d\omega \sigma \rho_{c,\sigma}(\omega), \quad (\text{A.75})$$

$$\tilde{m}_f = \sum_i i \langle f_i^{\dagger} f_i \rangle = \sum_i i \int d\omega \rho_{f,i}(\omega). \quad (\text{A.76})$$

For the gap equation we take symmetrized spectral function $A_{c\sigma;fi} = -\frac{1}{2\pi} [\text{Im}G_{c\sigma;fi}(\omega + i\delta) + \text{Im}G_{fi;c\sigma}(\omega + i\delta)] = \rho_{c\sigma;fi}$, where $G_{c\sigma;fi}(z) = \langle \langle c_{\sigma}^{\dagger}; f_i \rangle \rangle_z$, etc. For the evaluation of $\langle \chi_1 \rangle$ we will need two off-diagonal spectral functions:

$$\rho_{c\downarrow;f0} = \frac{J\chi_1}{\sqrt{3}(z - \lambda_0)} \rho_{c\downarrow}(\omega) \quad (\text{A.77})$$

$$\rho_{c\uparrow;f1} = \frac{\sqrt{2/3}J\chi_1}{z - \lambda_1} \rho_{c\uparrow}(\omega). \quad (\text{A.78})$$

The expectation value is

$$\langle \chi_1 \rangle = \frac{1}{2} [-\sqrt{1/3}(\langle c_{\downarrow}^{\dagger} f_0 + f_0^{\dagger} c_{\downarrow} \rangle) - \sqrt{2/3}(\langle c_{\uparrow}^{\dagger} f_1 + f_1^{\dagger} c_{\uparrow} \rangle)] = -\sqrt{1/3} \int A_{c\downarrow,f0}(\omega) d\omega - \sqrt{2/3} \int A_{c\uparrow,f1}(\omega) d\omega \quad (\text{A.79})$$

$$= -\sqrt{1/3} \frac{J\chi_1}{\sqrt{3}} \int d\omega \rho_{c\downarrow}/(\omega - \lambda_0) - \sqrt{2/3} \sqrt{2/3} J\chi_1 \int d\omega \rho_{c\uparrow}/(\omega - \lambda_1) \quad (\text{A.80})$$

$$= -(J\chi_1/3) \left[\int d\omega \rho_{c,\downarrow}(\omega)/(\omega - \lambda_0) \right] - 2J\chi_1/3 \left[\int d\omega \rho_{c\uparrow}(\omega)/(\omega - \lambda_1) \right]. \quad (\text{A.81})$$

Finally, we obtain the gap equation:

$$\boxed{\int d\omega \rho_{c\downarrow}(\omega)/(\omega - \lambda_0) + 2 \int d\omega \rho_{c\uparrow}(\omega)/(\omega - \lambda_1) = -3/J.} \quad (\text{A.82})$$

This equation has essentially the same structure as the gap equation for the $S = 1/2$ case.

Evaluation of energy

The total energy can be evaluated in analogy to the $S = 1/2$ case. We find

$$\frac{K_{\text{GS}}}{N} = E_0 + \sum_{\sigma} \int_{-\infty}^{\mu} d\omega (\omega - \mu) [\rho_{c,\sigma}(\omega) + \rho_{f,i(\sigma)}(\omega)] + (\lambda_{-1} - \mu) \theta(\omega - \lambda_{-1}) \quad (\text{A.83})$$

We evaluate Eq. A.83 for two different cases represented on Fig. 7. For case I, $E_c = \rho_{c,0} \sum_{\sigma} [(\mu^2 - \omega_{1,\sigma}^2)/2] - \mu n_c$, thus

$$\frac{K_{GS}}{N} = \rho_{c,0} \sum_{\sigma} [(\mu^2 - \omega_{1,\sigma}^2)/2] + \lambda(n_{f0} + n_{f1}) - \mu(n_f + n_c) \quad (\text{A.84})$$

In the case II,

$$E_c = \rho_c^0 \left(\frac{\mu^2 - \omega_{1,\downarrow}^2}{2} + \frac{\omega_{2,\uparrow}^2 - \omega_{1,\uparrow}^2}{2} \right) - \mu n_c. \quad (\text{A.85})$$

Phase diagrams for $S = 1/2$ and $S = 1$

We now discuss the different possible mean-field phases for the $S = 1/2$ and $S = 1$ Kondo lattice models.

One possible phase is a pure saturated ferromagnetic phase with magnetization $m_f = -g_f \mu_B S$ and with zero hybridisation, $\chi_{d,1} = 0$. If conducting electrons are completely polarized we call it the polar phase and the magnetization of conducting electrons is then given by

$$m_{c,P-I} = \mu_B g_c n_c / 2. \quad (\text{A.86})$$

For intermediate coupling regime, we distinguish between the ferromagnetic phases I, II, and III, which all have a finite value of the hybridisation parameter $\chi_{d,1}$ (thus a spectral gap). They are schematically represented in in Fig. 7. The phase I with the electron pockets, corresponds to the phase B' in the DMFT calculations. The phase II with the chemical potential in the gap corresponds to the DMFT phase A. The numerical results in the phase II clearly indicate that as we lower J the transition into phase III is expected, but when $\mu > \omega_{3,\uparrow}$ we were not able to find convergent solution in the regime of small J , as marked by the the dashed line in Fig. 8, see also [2]. This phase III would correspond to the phase B in the DMFT calculations, where this is a stable phase.

The phase boundary between the phase I and II or between the phase II and III is given by the condition

$$\tilde{m}_c + \tilde{m}_f = (2S - n)/2, \quad (\text{A.87})$$

for the expectation values of spin z component, which shows plateau behaviour irrespective of the Landé factors or, equivalently,

$$m_c/g_c + m_f/g_f = -\mu_B(2S - n)/2. \quad (\text{A.88})$$

This is equivalent to the condition that

$$\mu = \omega_{2(3),\uparrow} \quad (\text{A.89})$$

for transition between the phases I \rightarrow II (II \rightarrow III).

The pure Kondo singlet (paramagnetic) phase is defined by $m_c = 0, m_f = 0, \chi_{d,1} \neq 0$. We only find it for $S = 1/2$. In the $S = 1$ model the hole pocket never emerges; instead, the chemical potential becomes attached near the top of the bottom band for large J . In fact, similar behavior is also observed in the DMFT solutions. The boundary between phase I and the Kondo phase is determined by the condition

$$m_f = m_c = 0. \quad (\text{A.90})$$

The boundary between the phases I,II and polar-I is given by the condition

$$\chi_{d,1} = 0. \quad (\text{A.91})$$

We conclude that the qualitative features of the static MF and DMFT phase diagrams are rather similar, except that in the static mean-field theory the phase III is not stable. The main difference compared to previous works [2–4] is the finding that in the MF treatment the metamagnetic transition is described by the transition I \rightarrow II, while in the DMFT there are two different scenarios for metamagnetic transitions, either the transition I \rightarrow II or the transition II \rightarrow III, where only the former is expected for physically relevant model parameters.

-
- [1] K. S. D. Beach, eprint arXiv:cond-mat/0509778 (2005), arXiv:cond-mat/0509778 .
 - [2] S. Viola Kusminskiy, K. Beach, A. Castro Neto, and D. Campbell, Physical Review B, **77**, 094419 (2008).
 - [3] G.-B. Li and G.-M. Zhang, Physical Review B, **81**, 094420 (2010).
 - [4] K. Beach, P. Lee, and P. Monthoux, Physical Review Letters, **92**, 026401 (2004).

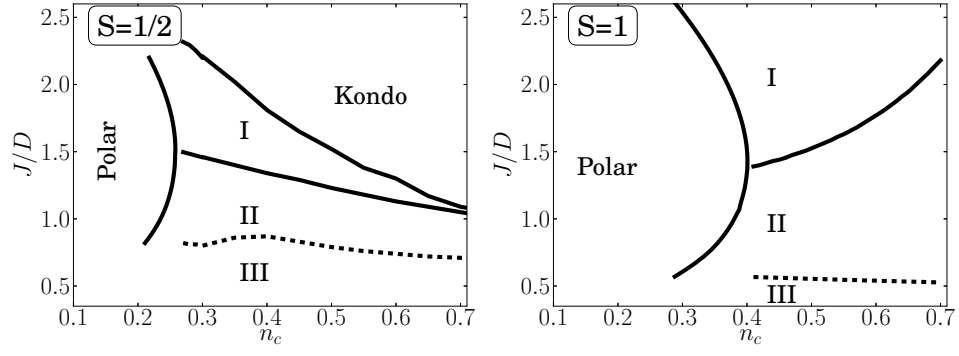


Figure 8: Ground state phase diagram of the KLM: (a) $S = 1/2$, (b) $S = 1$ with Landé factors $g_c = g_f = 1$. For the description of phases I, II, see the discussion in the text and Fig. 7. Phase Polar-I represent polarized phase with zero hybridisation and Kondo phase is paramagnetic phase ($m_c = m_f = 0$). The dashed line represent the transition into phase where we could not find the convergent solution, but phase III is expected, see discussion in the text.